Journal of the Brazilian Society of Mechanical Sciences and Engineering (2024) 46:286
https://doi.org/10.1007/s40430-024-04859-1

TECHNICAL PAPER

Structural design and characteristic analysis of three-oil port axial piston pump

Junpeng Feng[1] · Jun Wang[1] · Wentao Zhou[2] · Chuan Zeng[2] · Kongshuo Chu[1]

Received: 6 October 2023 / Accepted: 12 March 2024 / Published online: 7 April 2024

Abstract
Aiming at the problem that the flow rate of the two cavities of the differential cylinder does not match and it is not easy to achieve pump control, the team proposed the asymmetrical distribution principle of the axial piston pump with three ports, which can compensate for the flow difference between the two cavities of the differential cylinder without auxiliary components. Based on this principle, a new type of valve plate structure is designed by using the residual compression method. The pump performance is analyzed by PumpLinx simulation and experiment; the influence of the transition zone structure on the pressure and flow characteristics of the piston pump is researched. The basic characteristics of the pump such as pressure, flow, and noise under different working conditions were tested on the experimental platform, and the rationality of the new structure was verified. The new flow distribution scheme can not only compensate the flow difference of the differential cylinder, but also output two different pressures, which realizes the ideal effect of the hydraulic pump directly controlling the differential cylinder. The research work lays a theoretical foundation for the realization of the pump-controlled volumetric direct drive system.

Keywords Three-oil port axial piston pump · Flow distribution mechanism · Residual compression method · Pressure flow characteristics

1 Introduction

The pump-controlled volumetric direct drive system uses the hydraulic pump to directly provide the flow and pressure required by the system, drives the movement of the actuator, fundamentally reduces the throttling loss in the main circuit system, has the outstanding advantages of high efficiency, and reduces the heat of the system at the same time, which is the most direct and effective way to improve the energy efficiency of the hydraulic system, and is also the development direction of the hydraulic transmission system in future. However, for the widely used differential cylinder, because the inlet and outlet area of all the current hydraulic pumps is the same, the two cavities flow rate of the differential cylinder does not match, and it is not easy to realize pump control. Therefore, how to compensate for the differential flow the differential cylinder has become the key to realize the pump-controlled volumetric direct drive system. In order to balance of the flow of the differential cylinder, more additional components are used. Ahmed Imam [1, 2] proposed that two pilot-controlled check valves are used next to the throttle valve to compensate for the differential flow. The compensation valve only provides limited throttle in the critical working area, but the problem of throttle loss of the valve still exists. Lasse Schmidt [3] proposed a method of directly driving the differential cylinder by frequency conversion differential pump, using an electric rotating driver, whose shaft is connected to three fixed displacement gear pumps in opposite directions, so as to drive the differential cylinder, but the strategy is over the degree drive, the energy loss is large. Gustavo Koury Costa [4, 5] proposed three reversing valves to solve the flow mismatch problem, in which two directional valves are placed between the memory output and the circuit to compensate for the flow asymmetry, but fail to solve the throttle loss of

Technical Editor: Daniel Onofre de Almeida Cruz.

Jun Wang
wangjun01@tyut.edu.cn

1 College of Mechanical and Vehicle Engineering, Taiyuan University of Technology, Taiyuan 030024, China

2 Sichuan Chuanrun Hydraulic Lubrication Equipment Corporation, Chengdu 611743, China

the valve problem. Pedersen [6] proposed that through the use of digital displacement technology to achieve the direct flow control of the pump, in which the high-pressure valve controls the flow in and out of the high-pressure pipe, while the low-pressure valve controls the flow in and out of the low-pressure pipe, but restricted by the feedback control, the performance is worse than expected.

The above measures can achieve the purpose of compensating the flow imbalance of the differential cylinder, but the system becomes more complex. In order to solve this problem, our team proposed to use the three-port flow distribution method to control the differential cylinder in the axial piston pump, which can compensate for the flow difference of the differential cylinder without auxiliary components. Based on the residual compression method, this paper design the valve plate structure and verifies the structure by simulation and experiment.

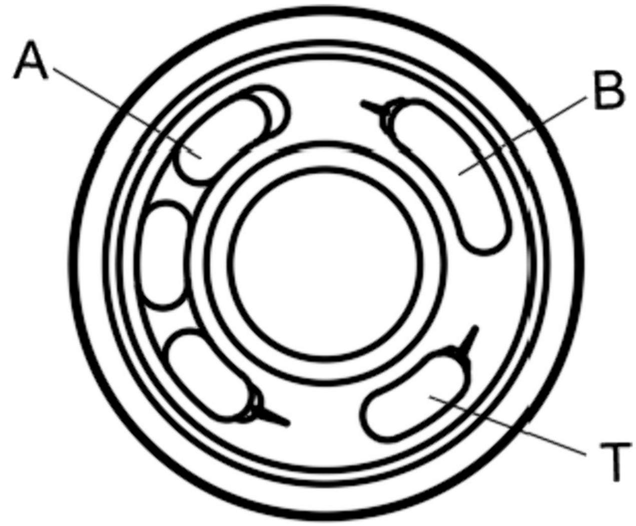

Fig. 2 New valve plate structure

2 New valve plate structure

According to the characteristics of the rotary flow distribution of the axial piston pump, the two-port flow distribution of the traditional valve plate (Fig. 1) is changed to three-ports [7, 8]. As shown in Fig. 2, the port A is connected to the rodless cavity of the differential cylinder, the port B is connected to the free rod cavity, and the port T is connected to the accumulator or tank. When the piston is rotated, the oil is absorbed once and the oil is discharged twice, or the oil is absorbed twice and the oil is discharged once [9, 10]. Under the premise of no additional auxiliary measures, the pump-controlled differential cylinder system is realized, which not only reduces the throttling loss but also simplifies the system structure. The new axial piston pump can also output different pressures through B and T ports to control two actuators, which has a good prospect of application.

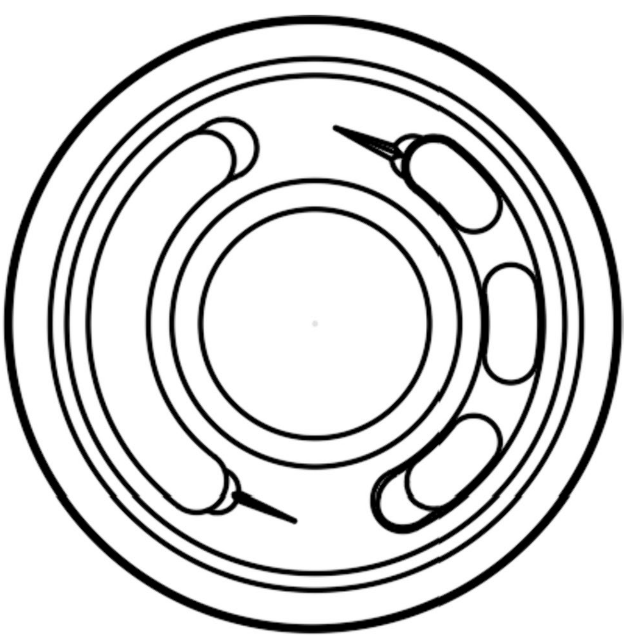

Fig. 1 Traditional valve plate structure

2.1 Study on the mechanism of flow distribution

In order to compensate the differential cylinder flow difference directly, the valve plate structure needs to be redesigned. According to the required flow of the two cavities of the differential cylinder and the oil suction and discharge flow of the piston pump A and B, the matching mechanism of the distribution envelope angle of the three-oil port axial piston pump A and port B with the differential cylinder is determined [11, 12], as shown in Eq. (1):

$$\frac{\left[1-\cos\left(\alpha_A+\theta\right)\right]\left[1-\tan\beta\tan\gamma\cos\left(\alpha_A+\theta\right)\right]}{\left[1-\cos\left(\alpha_B+\theta\right)\right]\left[1-\tan\beta\tan\gamma\cos\left(\alpha_B+\theta\right)\right]}=\frac{1}{a} \tag{1}$$

where

α_A is the port wrap angle of A;

α_B is the port wrap angle of B;

γ is the dip angle of piston;

β is the dip angle of swash plate;

θ is the wrap angle of the distribution port at the bottom of the cylinder block;

a is the area ratio of roded cavity to rodless cavity.

2.2 The residual compression method

In order to reduce leakage at the secondary part of the valve, improve the volumetric efficiency of the pump, ensure good lubrication, and avoid the occurrence of the burning plate, the residual compression method is used to design the structure of the valve plate.

2.2.1 Compaction force and torque

Due to the pressure action of high-pressure oil at the bottom of the piston cavity, the cylinder block is close to the side of the valve plate, so that the valve plate is affected by the axial pressing force of the cylinder block. The pressing force on the cylinder block is superimposed by the axial pressing force of the piston in the pressing oil zone, and the number of the piston in the pressing oil zone changes constantly with the change of the cylinder Angle φ, so a single piston is analyzed first. As shown in Fig. 3.

For the conical cylinder block, the axial pressing force F_z of a single piston is related to the inclination γ.

$$F_z = \frac{\pi d^2}{4} P_d \cos\gamma \tag{2}$$

Since the axial pressing force is parallel to the z-axis, only the torque of the x- and y-axis is generated [13], and the torque of the x- and y-axis is, respectively

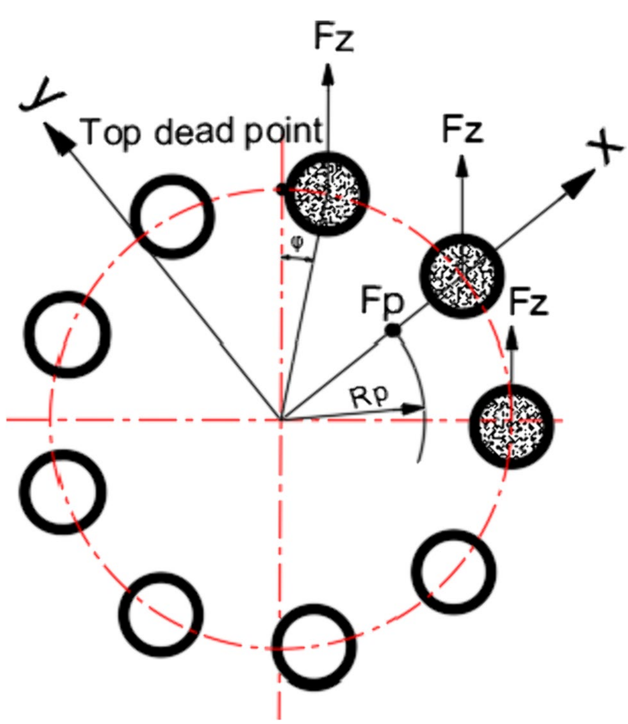

Fig. 3 Position of the action point of the pressing force

$$M_x = F_z y M_y = F_z x \tag{3}$$

$$x = L_{3k} \cos\theta_k \sin\gamma + R\cos\theta_k \tag{4}$$

$$y = L_{3k} \sin\theta_k \sin\gamma + R\sin\theta_k \tag{5}$$

$$L_{3k} = \frac{R\cos\theta_k \tan\beta + L_1}{\cos\gamma - \cos\theta_k \sin\gamma \tan\beta} \tag{6}$$

$$\theta_k = \varphi + 40^\circ(k-1) \tag{7}$$

The resulting axial pressing force of the piston in the oil pressing zone is the pressing force on the cylinder block

$$F_p = z_i F_z \tag{8}$$

The torque of the pressing force on the cylinder to the x-axis

$$M_x = F_z y_1 + F_z y_2 + \ldots F_z y_i \tag{9}$$

The torque of the pressing force on the cylinder to the y-axis

$$M_y = F_z x_1 + F_z x_2 + \ldots F_z x_i \tag{10}$$

Resultant moment

$$M = \sqrt{M_x^2 + M_y^2} = F_p R_p \tag{11}$$

where

d is the diameter of the piston;

P_d is the pressure of the high-pressure piston cavity;

R is the radius of dividing circle of the waist groove;

L_1 is the distance from the center of the plane where the piston ball center is located to the center of the cylinder bottom;

θ_k is the angular position of the k-piston, marking the first dead center piston and the second near port B;

z_i is the number of pistons in the oil pressure zone.

Because the number and position of the piston in the oil pressure area change with the angle of the cylinder block, the size of the pressing force, the application point, and the moment also change with the angle.

2.2.2 Support force and torque

The hydraulic support force F_0 is made up of three parts: The hydraulic support force of the outer seal with the hydraulic support force, the hydraulic support force of the inner seal with the hydraulic support force and the hydraulic support force of the high pressure oil of the oil port on the cylinder block.

$$F_0=\int_{R_2}^{R_3}P_d\phi r\mathrm{d}r+\int_{R_1}^{R_2}P_d\frac{\ln(r/R_1)}{\ln(R_2/R_1)}\phi r\mathrm{d}r+\int_{R_3}^{R_4}P_d\frac{\ln(R_4/r)}{\ln(R_4/R_3)}\phi r\mathrm{d}r \\ =\frac{\phi}{4}P_d\left(\frac{R_4^2-R_3^2}{\ln(R_4/R_3)}-\frac{R_2^2-R_1^2}{\ln(R_2/R_1)}\right) \tag{12}$$

The pressure wrap angle ϕ in Fig. 4 is made up of two parts [14]: The B distribution port and the distribution port on the bottom face of the cylinder block. The shaded part is a waist-shaped distribution port on the bottom face of the cylinder block. It can be seen from the symmetry that the position of action of the supporting force F_0 must be on the bisector of ϕ angle. The coordinate system is established with the center of the circle as the origin and the bisector of the pressure envelope angle as the x-axis. The radius of action of the supporting force is assumed to be R_0, which is obtained from the principle of the resultant moment.

$$M_y=F_0R_0=M_{y1}+M_{y2}+M_{y3} \tag{13}$$

$$M_{y1}=2\int_0^{\frac{\phi}{2}}\int_{R_3}^{R_4}\mathrm{p}r^2\mathrm{d}\varphi\mathrm{d}r\cos\varphi \tag{14}$$

$$M_{y2}=2P_d\left(\frac{R_1^3-R_2^3}{9\ln(R_2/R_1)}+\frac{R_2^3}{3}\right)\sin\frac{\phi}{2} \tag{15}$$

$$M_{y3}=2P_d\left(\frac{R_3^3-R_2^3}{3}\right)\sin\frac{\phi}{2} \tag{16}$$

Substitute F_0, M_{y1}, M_{y2}, M_{y3} into Eq. (13) to obtain the supporting force radius.

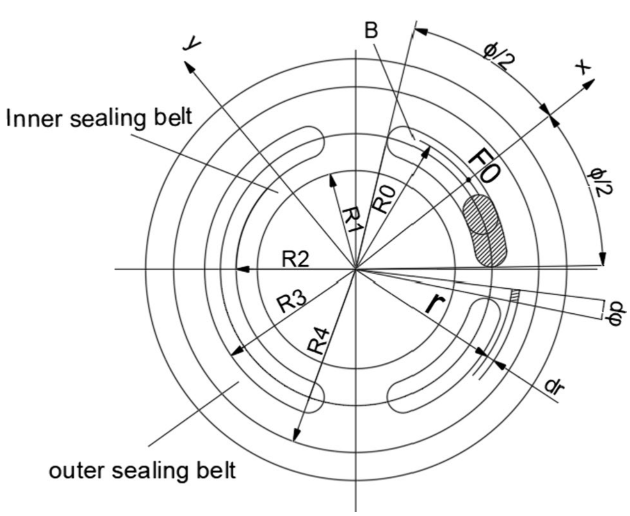

Fig. 4 Distribution of hydraulic support force of the valve plate

$$R_0=\frac{8}{9\phi}\left(\frac{(R_4^3-R_3^3)\ln(R_2/R_1)-(R_2^3-R_1^3)\ln(R_4/R_3)}{(R_4^2-R_3^2)\ln(R_2/R_1)-(R_2^2-R_1^2)\ln(R_4/R_3)}\right)\sin\frac{\phi}{2} \tag{17}$$

where

R_1 is the inner radius of the inner sealing belt;

R_2 is the outer radius of the inner sealing belt;

R_3 is the inner radius of the outer sealing belt;

R_4 is the outer radius of the outer sealing belt;

M_y is the torque of F_0 on the y-axis;

M_{y1} is the torque of the hydraulic pressure in the outer sealing belt to the y-axis;

M_{y2} is the torque of the hydraulic pressure in the inner sealing belt to the y-axis;

M_{y3} is the torque to the y-axis of the hydraulic support force resulting from the oil pressure in the ϕ plate port at the envelope angle.

Because the wrap angle of the pressure zone changes with the rotation of the cylinder, the size and action point of the support force also change with the angle of rotation.

2.2.3 Force balance analysis

If $F_p \approx F_0$ can be made and the position is the same, then the cylinder body is in an ideal state of balance. Once the two lines of action do not coincide, it will inevitably produce a torque that causes the cylinder block to overturn. Since the movement of the cylinder block is periodically changed by $2\alpha=2\pi/z$, and 2α is the angle between two adjacent pistons, in this paper only one cycle is analyzed. According to the difference of the number of pistons in the oil pressure area and the pressure angle, the position of the pressing force and the supporting force of the valve plate of the three-oil port axial piston pump is divided into four stages, as shown in Fig. 5, where the shaded area represents the position of the piston in the oil pressing stage, and φ represents the angle of the cylinder block.

The cylinder body starts from the upper dead point and is divided into the following four stages:

When $0°<\varphi<8.5°$, the number of pistons in the oil pressure zone is three, the wrap angle is unchanged, and the pressing force and the supporting force track are synchronized;

When $8.5°\le\varphi<21°$, there are two pistons in the oil pressure zone, the wrap angle decreases continuously, and the operating point of the pressing force lags behind that of the supporting force $(21°-\varphi)/2$;

When $21°\le\varphi\le27.5°$, there are two pistons in the oil pressure zone, the wrap angle is unchanged and the tracks of the pressing force and the support force are synchronized.

When $27.5°<\varphi\le40°$, there are two pistons in the oil pressure region, the wrap angle continues to increase, and the operating point of the pressing force is ahead of the operating point of the supporting force $(\varphi-27.5°)/2$.

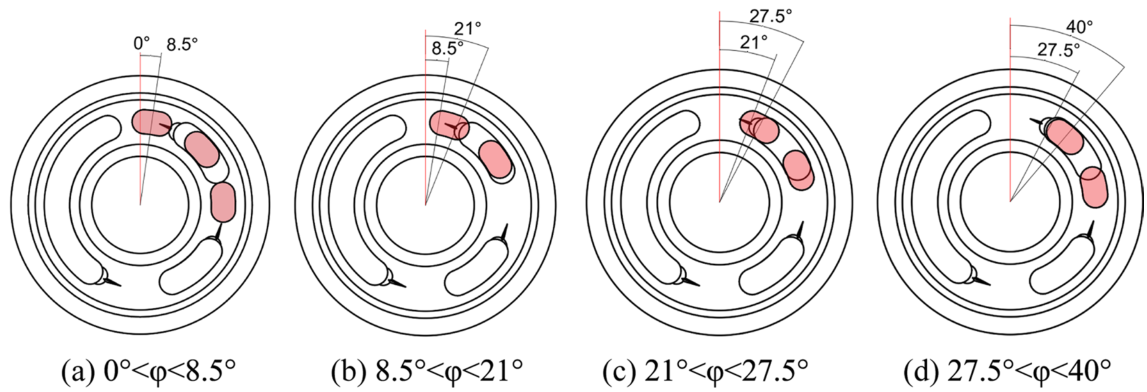

Fig. 5 Piston position diagram at different corners

In the first and third stages, the tracks of the pressing force and the supporting force are synchronized. In the second and fourth stages, the tracks of the operation points of F_0 and F_p are not synchronized, which will inevitably produce an overturning moment. To balance this overturning moment, the residual compression method is adopted; that is, the inverse moment formed by the residual compression force $\Delta F = F_p - F_0$ is used to balance its overturning moment. Keep the cylinder in balance. The calculation formula is

$$\varepsilon = \frac{F_p + F_s}{F_0} \tag{18}$$

where

F_s is the pre-pressing force of the center spring, generally 300 ~ 500 N, is also desirable (0.03 ~ 0.05) F_p;

ε is the pressing coefficient of the cylinder block on the valve plate, $\varepsilon = 1.05 \sim 1.10$ is recommended.

2.3 Transition zone design

In the design of the valve plate structure, the contradiction between the cylinder balance and the transient hydraulic shock caused by trapped oil is mainly solved, in order to prevent sudden expansion and pressing of oil, and at the same time to reduce noise and power loss. The method adopted in this paper is to set a triangular damping groove in the pre-compression angle, and through reasonable design of the triangular groove, the oil in the high- and low-pressure cavities can be gently converted, thus prolonging the time required for pressure conversion and achieving the purpose of reducing pressure pulsation. As shown in Fig. 6.

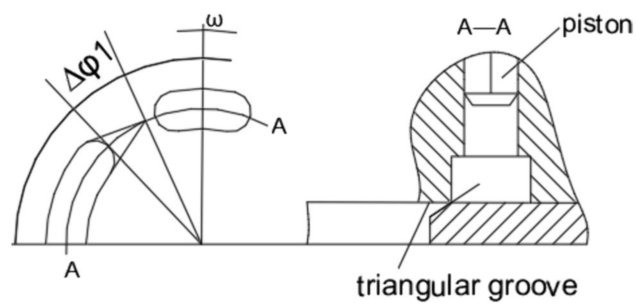

Fig. 6 Schematic diagram of the triangular groove structure

Due to the function of the triangular groove, the piston cavity in the upper dead center position is not immediately connected with the waist groove of the oil pressure port after the completion of oil absorption, but in the process of the cylinder body turning $\Delta\varphi_1$, the oil is continuously compressed by using the trapped oil in the piston cavity, and the pressure gradually rises to the pressure of the oil, and then, the pre-pressure boost process is completed. When the piston enters the low pressure area from the high pressure area, due to the movement of the piston, the volume of the piston cavity becomes larger, the oil in the cavity expands, and the pressure gradually decreases to achieve the purpose of pre-pressure relief. In this process, the displacement of the piston is proportional to the pressure of the oil.

For cone cylinder block, the piston movement position is determined by the rotation angle of the piston around the drive shaft, the inclination angle of the swash plate, and the inclination angle of the piston. The piston travel formula [15]

$$S = \frac{R_h \tan\gamma(1 - \cos\varphi)}{\cos\beta(1 - \tan\beta\tan\gamma\cos\varphi)} \tag{19}$$

In the upper dead center position, the oil pressing ΔV is the cavity content product change caused by the piston displacement Δx. If the oil volume in the piston cavity is V, the pressure rises from P_0 to P, and the corresponding cylinder block rotation angle $\Delta\varphi_1$ is satisfied.

$$\begin{aligned}\Delta V &= \frac{\pi d^2}{4}\Delta x\\ &= \frac{\pi d^2}{4}\frac{R_h \tan\gamma\left(1 - \cos\Delta\varphi_1\right)}{\cos\beta\left(1 - \tan\beta\tan\gamma\cos\Delta\varphi_1\right)}\end{aligned} \tag{20}$$

$$\Delta V = V\frac{P-P_0}{E} \tag{21}$$

$$V = V_0 + \frac{\pi d^2}{4}S_{\max} \tag{22}$$

At the bottom dead center position, the pressure drops from P to P_0, and the volume in the piston cavity, that is, the residual volume is V_0, then $V=V_0$ in Eq. (22) corresponds to the rotation angle $\Delta\varphi_2$ of the cylinder block.

At the nondead point, the pressure decreases from P_b to P_t corresponding to the pressing volume V_1, corresponding to the cylinder block rotation angle $\Delta\varphi_3$.

$$V_1 = V_0 + \frac{\pi d^2}{4}S_1 \tag{23}$$

$$S_1 = S_{\max} - \frac{R_h \tan\gamma(1-\cos 99.25°)}{\cos\beta(1-\tan\beta\tan\gamma\cos 99.25°)} \tag{24}$$

where

R_h is the distance from the center of the top dead center of the piston to the main shaft;

V_0 is the residual volume in the piston cavity at the bottom dead center;

P is the high and low cavity pressure;

P_0 is the high and low cavity pressure;

E is the modulus of elasticity of the working liquid.

At $dt = \Delta\varphi/\omega$ time, all the compressed liquid is introduced by the triangular groove [16]. As shown in Fig. 7.

$$Q\frac{\Delta\varphi}{\omega} = \Delta V \tag{25}$$

$$Q = C_d A\sqrt{\frac{(P-P_0)}{\rho}} \tag{26}$$

$$A = R^2\Delta\varphi^2\tan\theta_1\sin\theta_1\tan\frac{\theta_2}{2} \tag{27}$$

where

A is the flow area of the triangular groove;

θ_1 is the depth angle of the triangular groove;

θ_2 is the width angle of the triangular groove.

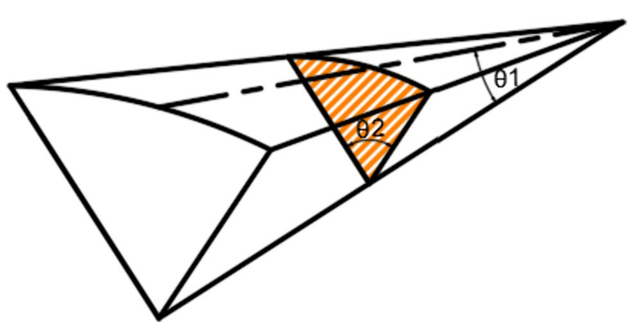

Fig. 7 Schematic diagram of the triangular groove section

Table 1 Valve plate structure parameters

Parameter	Numerical value
Area A wrap angle/°	138
Area B wrap angle/°	61
Area T wrap angle/°	41
Top dead point triangular groove wrap angle/°	11
Bottom dead point triangular groove wrap angle/°	14.5
Nondead point triangular groove wrap angle/°	12
Width of waist groove/mm	8.4

Through appeal calculation and analysis, the specific structural parameters of the valve plate are obtained as shown in Table 1.

3 Simulation analysis

In this paper, PumpLinx fluid simulation software is used to analyze the fluid model of the pump under different load conditions. Since the research object is a high-speed rotating axial piston pump, the high Reynolds number turbulence model, the standard k-ε model. For fluid simulation, high-quality mesh is often the basis for the correct operation of the simulation model, and dividing the mesh is not the more refined the better. In order to obtain the best flow field model of the simulation, different grid parameters are set for pre-simulation, and the grid sensitivity is analyzed by comparing the import and export flow error under each parameter. The flow error $\Delta Q\%$ is calculated as follows [17]:

$$\Delta Q\% = \frac{|Q_1-Q_2|}{Q_2}\cdot 100\% \tag{28}$$

where

Q_1 is the inlet flow rate;

Q_2 is the outlet flow rate.

Through comparative analysis, while fully considering the calculation time and accuracy, the parameter setting of each fluid domain grid is finally determined as shown in Table 2:

Figure 8 shows the flow field model inside the pump.

Figure 9 shows the pressure cloud diagram under the conditions of 20 MPa at port B and 5 Mpa in port T. As shown in Fig. 9b, when the piston passes through the nondead point transition zone, there is an obvious pressure rise phenomenon, and the pressure gradually decreases from the waist groove area to both sides in the same radial direction, and the pressure on the same circumference basically does not change.

In order to study the flow pressure characteristics of port B, the pressure of port T was set to 0 Mpa in the simulation

Table 2 Grid parameters

Parameter	Import and export basin	The piston basin	Valve plate basin	Spherical oil membrane basin
Critical edge angle/°	30	15	25	15
Curvature resolution/°	35	20	30	20
Maximum cell size	0.03	0.02	0.02	0.02
Minimum cell size	0.002	0.001	0.001	0.001
Cell size on surfaces	0.015	0.004	0.004	0.004

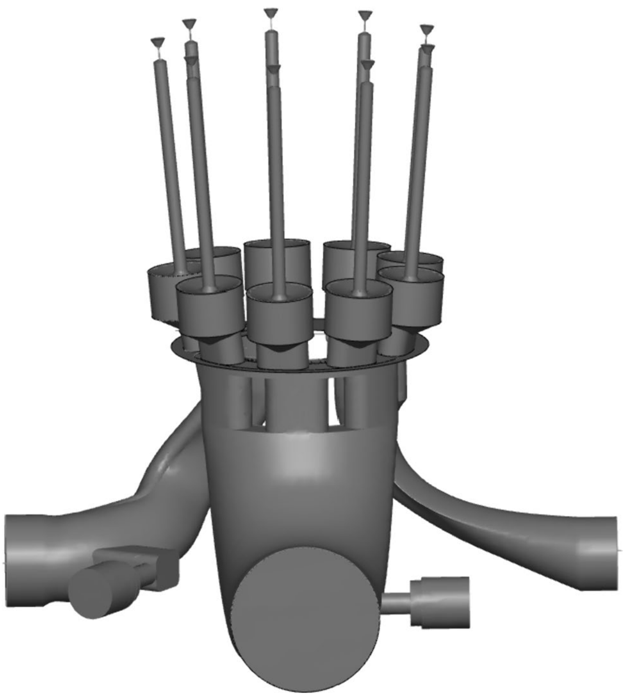

Fig. 8 Flow field model of three-oil port axial piston pump

process, and the pressure of port B was simulated under the working conditions of 5 Mpa, 10 Mpa and 20 Mpa, respectively. According to Fig. 10 of the simulation results, the flow pulsation pattern is consistent under different working conditions. Since the pressure pulsation is generated by the action of the flow pulsation, the law of the pressure pulsation is similar to that of the flow pulsation and the period is $2\pi/z$.

As shown in Fig. 10, with the increase of the pressure in port B, the output flow rate decreases, the pulsation amplitude of the flow decreases from 12.4 L/min to 8.8 L/min, and the flow pulsation rate also decreases from 43.1% to 31.9%. This is because part of the oil flows into the port T, and with the increase of the pressure difference between B and T, the pressure transition of the piston cavity is completed in advance, and the fluctuation peak value is reduced, so the flow pulsation amplitude and pulsation rate are reduced. The pressure pulsation is generated by the flow pulsation, so it also decreases. As shown in Fig. 11, the pressure pulsation rate decreases from 0.19% to 0.03%.

As shown in Fig. 12, in the transition zone B and T, the volume of the piston cavity is closed and compressed, resulting in a large positive overshoot of pressure. Pre-depressurized by the triangular groove reduces the overshoot. With increasing pressure at port B, the amplitude of pressure pulsation in the piston cavity decreases from 14.1 Mpa to 7.5 Mpa, and the pressure pulsation rate decreases to 37.4%.

Fig. 9 Pressure cloud of the three-oil port axial piston pump

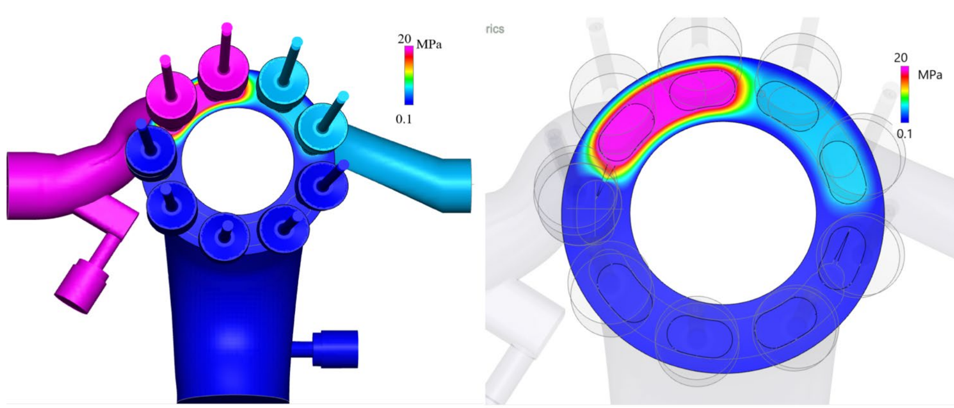

(a) piston pump (b) oil film

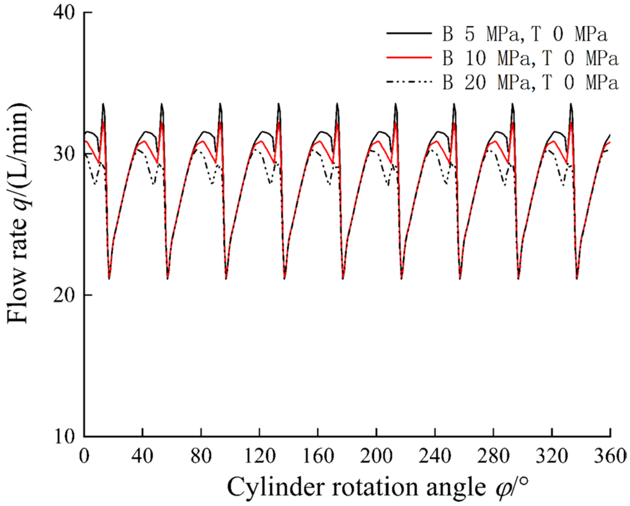

Fig. 10 B-port flow rate at a speed of 1500 r/min

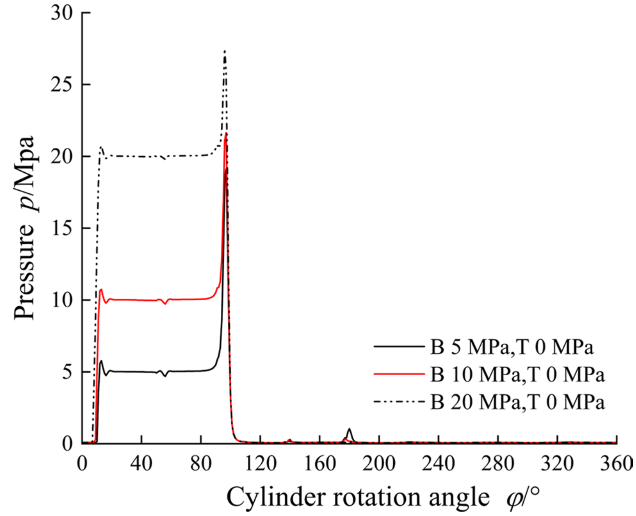

Fig. 12 Pressure in the piston cavity at a speed of 1500 r/min

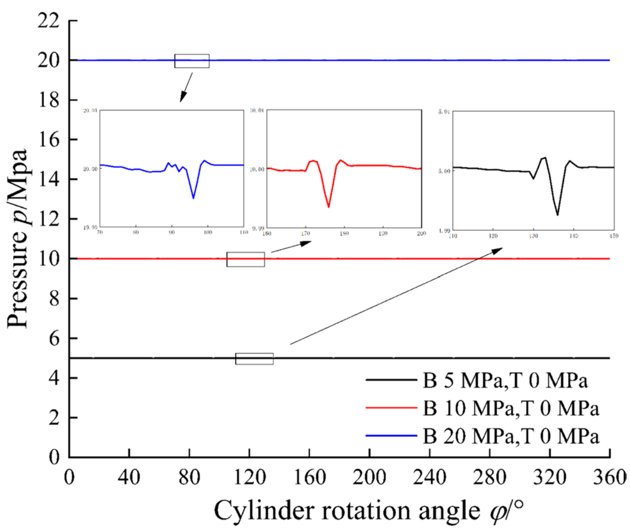

Fig. 11 B-port pressure at a speed of 1500 r/min

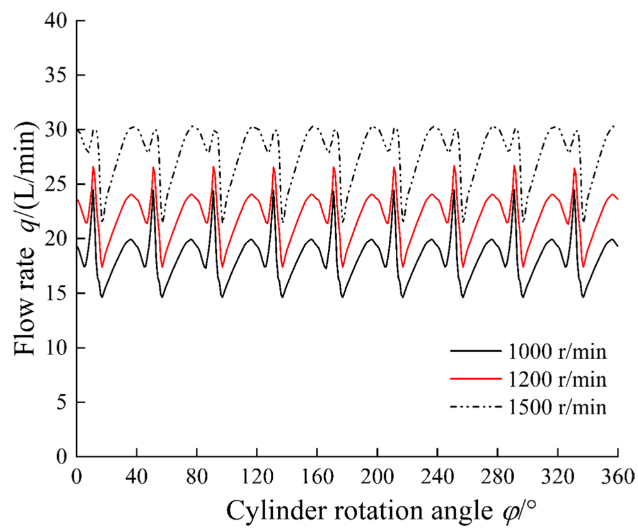

Fig. 13 Flow rate of B-port at different speeds

At the same time, the pressure impact generated by the piston cavity during the flow distribution process will react on the output pressure of port B, resulting in a relatively obvious pressure pulsation. Since the piston enters the high pressure oil discharge area of the valve plate, the oil in the piston cavity is connected to the oil at the B outlet of the pump, so the pressure change in the piston cavity and the pressure fluctuation at the pump outlet will interact.

Figures 13, 14 and 15, respectively, show the flow rate, pressure, and pressure in the B-port at different speeds. The analysis shows that with the increase in speed, the pulsation period decreases and the output flow rate at B-port increases. The output pressure remained basically unchanged and the pressure pulsation rate remained at 0.03%.

As can be seen in Fig. 13, with the increase in rotational speed, the amplitude of flow pulsation at outlet B decreases from 9.8 L/min to 8.9 L/min, and the flow pulsation rate decreases from 53.8% to 32.1%. This is due to the increase in speed, resulting in the piston in the B, T transition interval of the flow time becomes shorter, the pre-depressurization process is not sufficient, the flow into T through the triangular groove decreases, the peak fluctuation decreases. At the same time, because of the increase of the pump spindle speed, the average output flow rate of the pump also increases, so the flow pulsation rate decreases.

As shown in Fig. 15, with the increase in rotational speed, the amplitude of piston pressure pulsation increases from 1.8 Mpa to 8.5 Mpa and the piston pressure pulsation rate

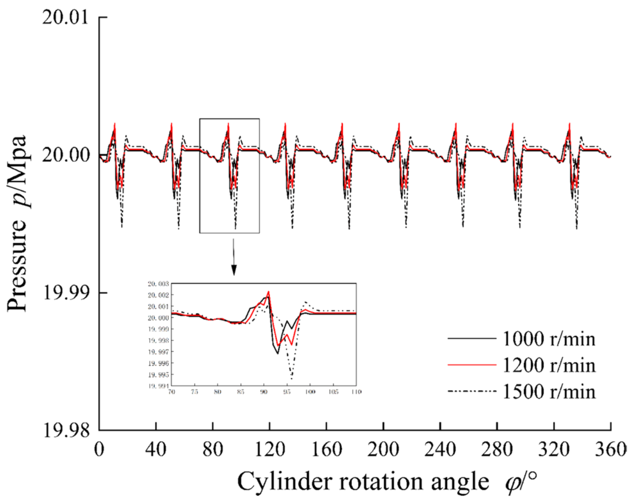

Fig. 14 Pressure of B-port at different speeds

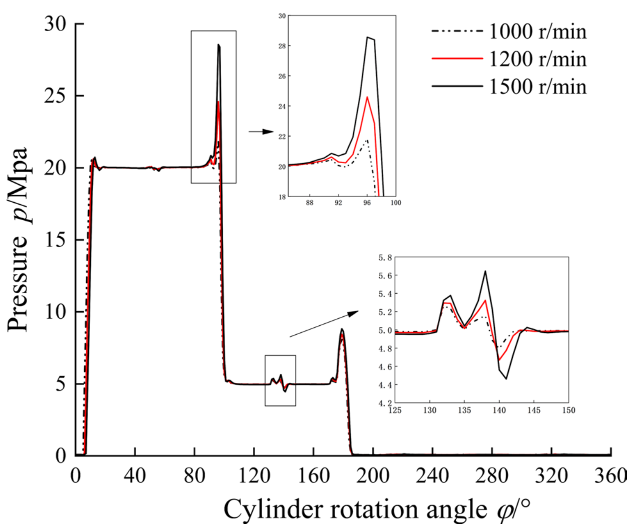

Fig. 15 The pressure in the piston cavity at different speeds

increases from 9.1% to 42.8%. This is due to the flow distribution time of the piston in the transition interval becomes shorter, resulting in trapped oil causing the pressure impact inside the piston cavity to increase.

4 Experimental verification

The test platform was designed and built according to the distribution characteristics of the axial piston pump with three-oil ports. Figure 16 shows the test bench for prototype testing, and Fig. 17 shows the valve plate.

The oil port B and oil port T are loaded by the relief valve, and two pressure flow sensors are connected to collect pressure flow data. The frequency converter is used to control the speed of the motor. By controlling the motor speed and load pressure, the characteristics of port flow and pressure B and T are tested. Considering the large variation range of flow, the test adopts QT 510 turbine flowmeter, the working range is 2.0–75 L/min, the output signal frequency can reach 30 kHz, and the measurement error is less than 0.5%. Because the test condition is high pressure, the PR110 model pressure sensor with a working range of 0–40 Mpa is selected, and the measurement error is less than 1 ms. In order to avoid the interference of noise to the test, the paper effectively solves most of the interference problems by grounding the shielding body and effectively surrounding the circuit elements into a cylindrical shielding cover. At the same time, in order to ensure the sampling accuracy, the sampling frequency is 1000 Hz.

Set the angle of tilt of the swash plate to 15° and the pump speed at 1500 r/min to load the pressure of port B. When the loading pressure is 5, 10 and 20 MPa, the port B-pressure flow test results are shown in Figs. 18 and 19. As can be seen in Fig. 18, the pressure pulsation of port B decreases with the increase in pressure. The total pulsation amplitude is 0.5 Mpa, and the pressure pulsation rate is 2.5%, indicating good performance of the piston pump.

According to the analysis of Fig. 19, with the increase in pressure, the average output flow of port B decreases from 31.9 L/min to 28.5 L/min. This is due to the increase in load pressure, resulting in the leakage of three pairs of friction pairs, that is, the gap between the cylinder and the valve plate, between the cylinder and the piston and between the slide boot and the swash plate increases, so the output flow decreases. On the other hand, with the increase in pressure, the pressure transition is completed in advance, the peak pulsation decreases, and the average output flow decreases, so the flow pulsation amplitude and flow pulsation rate decrease.

In order to facilitate the calculation accuracy of the simulation, the following analysis is made in Table 3. According to Table 3, Fig. 10 simulation results are 2.5% ~ 8.3% error compared with the experiment.

At the same time, in order to study the influence of the spindle speed on the pump volume efficiency, the paper uses the measuring cylinder to measure the leakage per unit time. The specific measurement data are shown in Table 4.

According to the measurement data in Table 4, the volumetric efficiency of the pump under different working conditions can be calculated. To facilitate the analysis, the dot and line diagram shown in Fig. 20 is made. As can be seen in Fig. 20, when the load pressure is constant, the volumetric efficiency of the piston pump increases with the increase in the rotational speed. When the load pressure is 20 Mpa, the speed has a great influence on the volumetric efficiency. With the increase in the speed, the volumetric efficiency increases from 98.9% to 99.4%. When the load

Fig. 16 Test bench

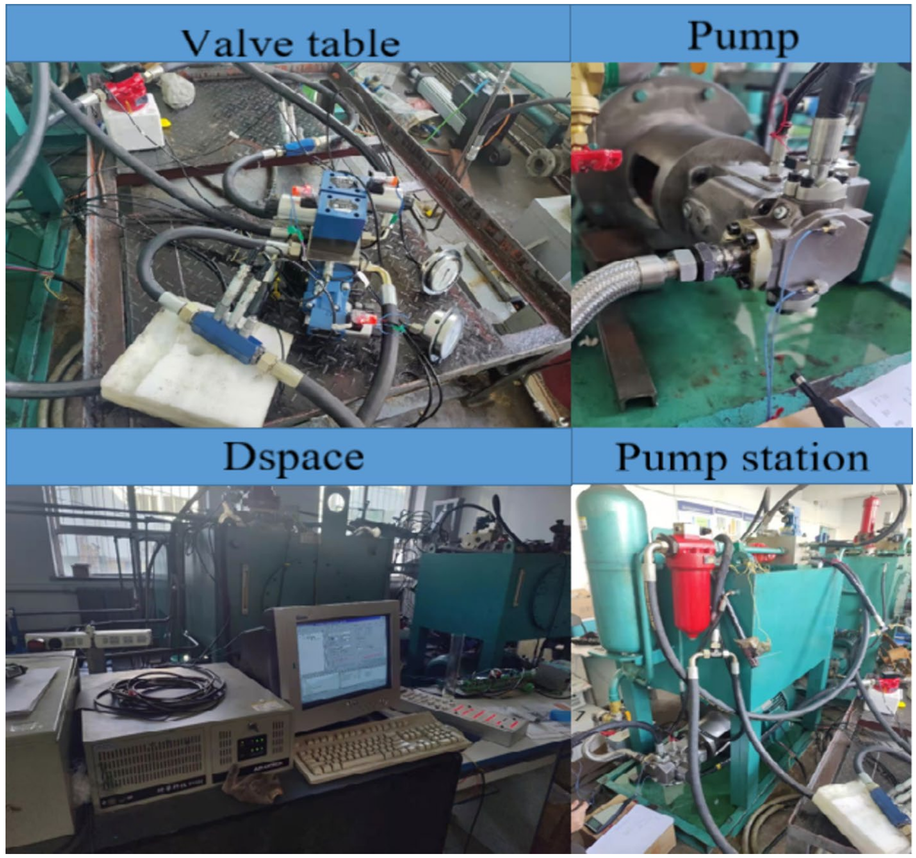

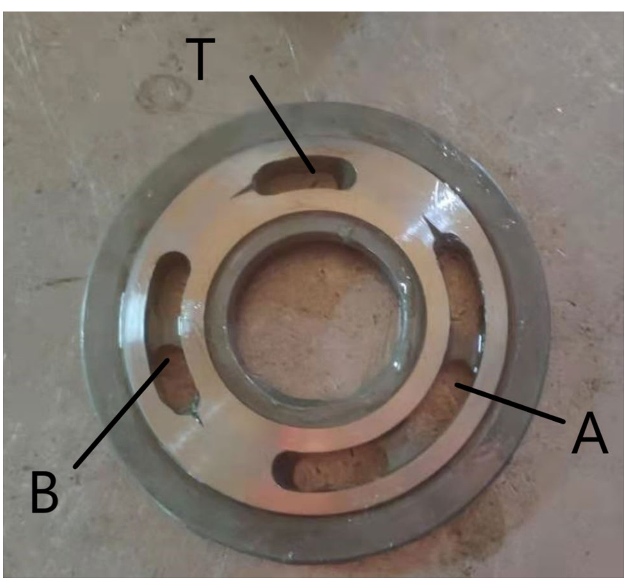

Fig. 17 Valve plate

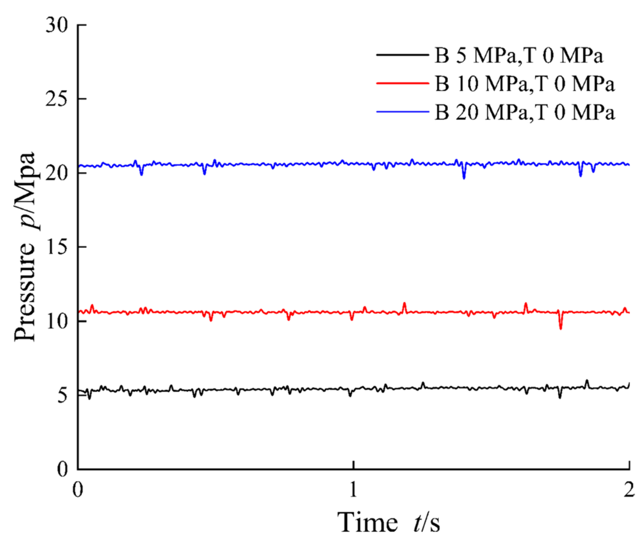

Fig. 18 B-port pressure

pressure is 5 and 10 Mpa, the speed has little effect on volumetric efficiency, and volumetric efficiency increases from 99.6% to 99.7%, basically no change.

When the speed is constant, the volumetric efficiency of the piston pump decreases with the increase in the load pressure. This is due to the increase in pressure, resulting in an increase in the leakage of the three pairs of friction pairs, that is, between the cylinder block and the valve plate,

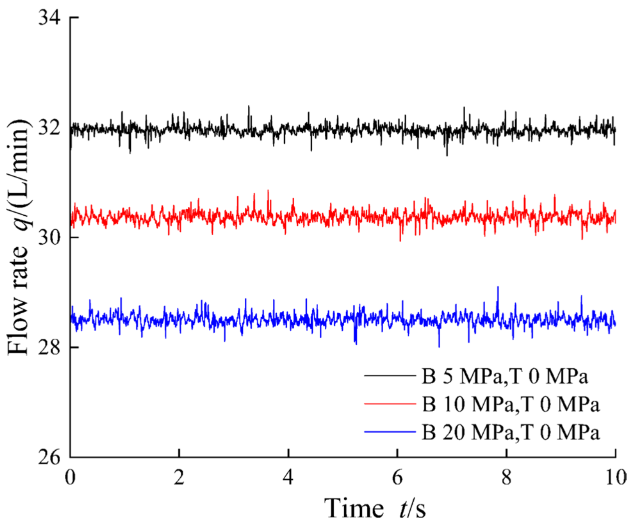

Fig. 19 B-port flow rate

Table 3 Error of the average output flow rate

B-port pressure/Mpa	Experimental average output flow rate/(L/min)	Simulation of the average output flow rate/(L/min)	Error/%
5	31.4	28.8	8.3
10	30.4	28.4	6.5
20	28.4	27.7	2.5

Table 4 Leakage under different working conditions

Main shaft speed/(r/min)	B 5 Mpa leakage/(mL/min)	B 10 MPa leakage/(mL/min)	B 20 MPa leakage/(mL/min)
600	79	97	260
700	80	111	284
800	90	126	296
900	101	141	304
1200	128	172	342
1500	150	195	380

between the cylinder block and the piston, and between the boot and the swash plate, so the volumetric efficiency is reduced.

The B and T ports of the three-oil port axial piston pump are loaded by adjusting the pilot relief valve. The test is carried out under the conditions of 20 MPa pressure at B port, 5 MPa pressure at port T and 1500 r/min motor speed. The experimental data are shown in Fig. 21. It can be seen from the curve in Fig. 21 that the flow pulsations at ports B and T match.

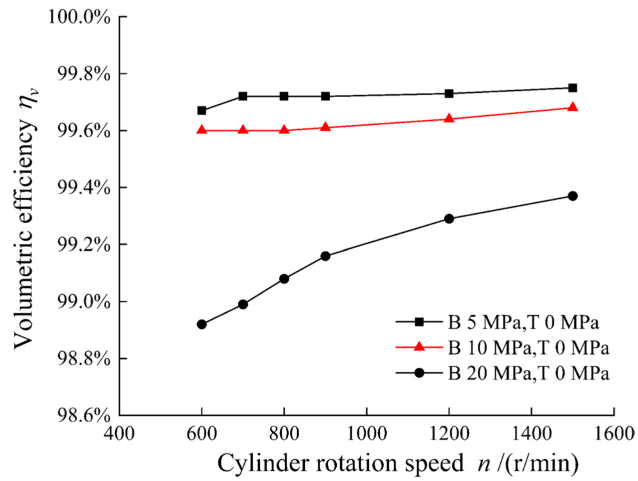

Fig. 20 Volumetric efficiency

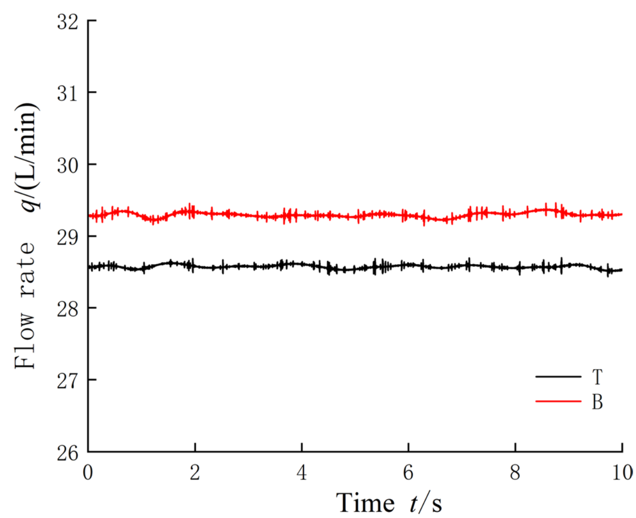

Fig. 21 Flow rate of B and T ports

From the above analysis, it can be seen that the pressure pulsation of the test pump is consistent with the phase of the flow pulsation mode, and the flow pulsation rate changes with the working conditions, but the overall stability is maintained between 0.4% and 1.5%. The error between the simulation output flow and the experiment is 2.5% ~ 8.3%. The test results further verify the accuracy of the simulation results and theoretical analysis.

5 Conclusions

The thesis mainly uses residual compression method to design the valve plate structure of the three-oil port axial piston pump. By simulation and experimental, the performance of the three-oil port axial piston pump is analyzed, and the conclusions are as follows:

(1) The new flow distribution principle is to compensate the asymmetric flow caused by the difference in the areas of the differential cylinder. Under different working conditions, the phase of pressure pulsation and flow pulsation vibration mode of the plate structure designed by the residual compression method is consistent, and the volumetric efficiency is maintained above 99%. Meanwhile, the damping structure of the transition zone is used to gently transform the oil in the high- and low-pressure cavity. The pressure pulsation amplitude is kept within 0.5 Mpa, which verifies the rationality of the theoretical design.
(2) The influence of the parameters of the piston pump on the flow pressure pulsation characteristics was analyzed by the method of flow field simulation and experimental verification, and the variation law of the flow pressure pulsation characteristics of the three-oil axial piston pump with the working parameters was revealed: The flow pressure pulsation amplitude and pulsation rate of the piston pump decreased with the increase in load pressure and speed. The pressure pulsation rate of the piston cavity increases with the increase in the speed and decreases with the increase in the pressure. The simulation results are consistent with the test results, which verifies the correctness of the theoretical model and the precision of the numerical simulation.

The new valve plate structure can realize differential compensation without additional auxiliary components. At the same time, it can output two different pressure flows and control the movement of different mechanisms, with the advantages of high energy efficiency, compact structure, and low cost, which provides a theoretical and practical basis for the realization of green hydraulic control technology.

Acknowledgements This paper is supported by the National Natural Science Foundation of China (Grant No.51905369).

References

1. Imam A, Rafiq M, Jalayeri E, Sepehri N (2018) A pump-controlled circuit for single-rod cylinders that incorporates limited throttling compensating valves. Actuators 7(2):13. https://doi.org/10.3390/act7020013
2. Imam A, Rafiq M, Jalayeri E, Sepehri N (2017) Design, implementation and evaluation of a pump-controlled circuit for single rod actuators. Actuators 6(1):10. https://doi.org/10.3390/act6010010
3. Schmidt L, Groenkjaer M, Pedersen HC, Andersen TO (2017) Position control of an over-actuated direct hydraulic cylinder drive. Control Eng Pract 64:1–14. https://doi.org/10.1016/j.conengprac.2017.04.003
4. Costa GK, Sepehri N (2020) A critical analysis of flow-compensated hydrostatic single rod actuators: simulation study. Actuators 9:58. https://doi.org/10.3390/act9030058
5. Costa GK, Sepehri N (2019) A critical analysis of valve-compensated hydrostatic actuators: qualitative investigation. Actuators 8(3):59. https://doi.org/10.3390/act8030059
6. Pn H, Per J, Lasse S et al (2020) Control and performance analysis of a digital direct hydraulic cylinder drive. Int J Fluid Power. https://doi.org/10.13052/ijfp1439-9776.2032
7. Quan L (2008) Current state, problems and the innovative solution of electro—hydraulic technology of pump controlled cylinder. Chin J Mech Eng 44(11):87–92. https://doi.org/10.3901/JME.2008.11.087
8. Jing J, Quan L, Huang JH et al (2016) Research on the characteristics of asymmetric pump directed controlled arm cylinder of excavator. Chin J Mech Eng 52(6):188–196. https://doi.org/10.3901/JME.2016.06.188
9. Zhang XG, Wang XY, Zhang HJ et al (2019) Characteristics of wheel loader lifting device based on closed pump-controlled three-chamber hydraulic cylinder. Trans Chin Soc Agric Mach 50(10):410–418. https://doi.org/10.6041/j.issn.1000-1298.2019.10.048
10. Gao YS, Cheng J, Huang JH, Quan L (2017) Simulation analysis and experiment of variable-displacement asymmetric axial piston pump. Appl Sci 7(4):328. https://doi.org/10.3390/app7040328
11. Xu B, Zhang JH, Yang HY, Ye SG (2013) Multi-objective drive forward design with damping orifice and groove for axial piston pump. Trans Chin Soc Agric Mach 44(7):279–285. https://doi.org/10.6041/j.issn.1000-1298.2013.07.048
12. Wang J, Wang JJ (2020) Research on asymmetric axial piston pump. Shanxi Metall 43(1):21–22. https://doi.org/10.16525/j.cnki.cn14-1167/tf.2020.01.07
13. Huang JH, He W, Hao HM et al (2019) Analysis of control characteristics of variable-displacement asymmetric axial piston pump. Trans Chin Soc Agric Mach 50(3):368–376. https://doi.org/10.6041/j.issn.1000-1298.2019.03.042
14. Li ZY (2011) Hydraulic components and systems. China Machine Press, Beijing
15. Huang MH, Wang ZZ, Pan Q et al (2022) Modeling simulation and characteristics analysis of pump control system of concrete pump truck. J South China Univ Technol (Natural Science Edition) 50(3):106–118. https://doi.org/10.12141/j.issn.1000-565X.210330
16. Ge L, Quan L, Li YW et al (2018) A novel hydraulic excavator boom driving system with high efficiency and potential energy regeneration capability. Energy Convers Manag 166:308–317. https://doi.org/10.1016/j.enconman.2018.04.046
17. Liu J, Zhao B, Gao GJ et al (2021) Consider the influence of viscosity-temperature characteristics on the cavitation jet of axial piston pump. Chin Hydraul Pneum 45(7):35–42. https://doi.org/10.11832/j.issn.1000-4858.2021.07.006